Journal of Advanced Research in Applied Sciences and Engineering Technology

Journal homepage:
https://semarakilmu.com.my/journals/index.php/applied_sciences_eng_tech/index
ISSN: 2462-1943

Fabrication Biowaste-Derived Carbon Quantum Dot/Calcium Oxide for Photodegradation of Methylene Blue under Visible Light

Sin Yuan Lai[1,*], Hongwei Dong[1], G. Abdulkareem-Alsultan[2], Mukhamad Nurhadi[3], Surya Lubis[4], Mahashanon Arumugam[5], Siti Najihah Md Hashim[6], Aqilah Fasihah Rusli[6], Rabiah Nizah Md Fahmy[6], Nur Dalila Mohamad[6], Mohd Zulhelmy Ahmad[6]

[1] School of Energy and Chemical Engineering, Xiamen University Malaysia, Jalan Sunsuria, Bandar Sunsuria, Selangor Darul Ehsan, 43900 Sepang, Selangor, Malaysia
[2] Catalysis Science and Technology Research Centre (PutraCat), Faculty of Science, Universiti Putra Malaysia, Serdang, Selangor 43400, Malaysia
[3] Department of Chemical Education, Universitas Mulawarman, Kampus Gunung Kelua, Samarinda, 75119, East Kalimantan, Indonesia.
[4] Department of Chemistry, Faculty of Mathematics and Natural Sciences, Universitas Syiah Kuala, Darussalam 23111, Banda Aceh, Indonesia
[5] Tomato Sustainables Ltd, Subsidiary of Senapt Ltd, R79, R71, RAL, STFC, Fermi Ave, Harwell, Didcot, Oxfordshire OX11 0QX, United Kingdom
[6] Laboratory Center, Xiamen University Malaysia, Jalan Sunsuria, Bandar Sunsuria, Selangor Darul Ehsan, 43900 Sepang, Selangor, Malaysia

ARTICLE INFO

Article history:
Received 13 December 2025
Received in revised form 19 February 2026
Accepted 15 April 2026
Available online 7 May 2026

Keywords:
Biowaste; Carbon quantum dot; Calcium oxide; Photodegradation; Wastewater treatment

ABSTRACT

In response to the significant environmental risks posed by the discharge of synthetic dyes into water bodies from the textile industry in Malaysia, this study presents a sustainable solution utilizing orange peel waste-derived carbon quantum dot (CQD) and calcium oxide (CaO) for the photodegradation of methylene blue (MB) under visible light. This approach not only addresses environmental contamination but also promotes the reuse of biowastes, aligning with circular economy principles and environmental sustainability. This research includes the CQD/CaO nanocomposites sourced from biomass wastes using a microwave-hydrothermal method, investigation on the dyes photodegradation efficiency under visible light, focusing on catalyst loadings and initial dye concentrations. Additionally, the kinetic studies and type of heterojunction were explored as well. Characterizations involve a range of techniques, including Fourier-transform infrared spectroscopy (FTIR), photoluminescence (PL) spectroscopy, and Diffuse reflectance ultraviolet-visible spectroscopy (DR UV-Vis). The CQD/CaO heterojunction significantly enhances photocatalytic efficiency by promoting charge separation and visible light absorption. PL analysis showed that the nanocomposite exhibits much lower PL intensity than pure CQD, indicating reduced electron-hole recombination. FTIR results confirm an increased surface hydrophilicity and the introduction of new hydroxyl groups, while UV-Vis analysis demonstrats a narrowed band gap and broader light absorption in the CQD/CaO nanocomposite. Together, these properties enable more efficient photodegradation of MB under visible-light illumination. Under optimized reaction conditions, specifically with a catalyst loading of 0.5 g/L, initial MB concentration of 15 ppm, at pH 7 and in the presence of 10 mL 5 mM H_2O_2, the CQD/CaO photocatalyst achieved a photodegradation efficiency of 72.61% within 3 hours of visible-light irradiation. The findings are expected to provide insights into the feasibility of deploying biowaste-derived materials for effective environmental remediation, offering a dual benefit of pollution reduction and waste management.

* *Corresponding author.*
E-mail address: sinyuan.lai@xmu.edu.my

1. Introduction

Malaysia's contemporary civilisation and economic progress rely heavily on its textile sector [1]. Over the past few decades, the sector has grown and developed quickly, which has led to the dumping of different pollutants in different locations. The textile industry has grown to be the one that processes wastewater the most both in Asia and globally. The textile industry uses over 10,000 different kinds of pigment and dyes, which adds up to almost 700,000 tonnes of synthetic colours produced annually [2]. The discharge of synthetic dyes into bodies of water constitutes a substantial hazard, resulting in environmental issues, such as threat to aquatic life and potential human health risks [3,4]. Current treatment methods are often inadequate, necessitating the exploration of sustainable, green, energy-efficient technologies. Photodegradation, which is one of the wastewater treatment methods, employs semiconductors that could generate reactive oxygen radicals to decompose the textile dyes [5]. This approach is renewable and sustainable because it uses sunlight as the energy source, and sunlight is naturally replenished every day. It often breaks down pollutants into simpler, less harmful substances.

In recent years, several low-cost and low-value biowastes, such as waste chicken eggshells [6-8], oil palm frond [9], palm kernel shells [10], and empty fruit bunches [4], citrus fruit peels [11], banana peels [12], and orange fruit peels [13,14], have been transformed into usable materials. These renewable waste materials are environmentally friendly and cost-effective. They have been utilized in textile photodegradation to mitigate the water contamination [4,6,9]. The waste chicken eggshells containing calcium materials such as calcium carbonates ($CaCO_3$), exhibits some noteworthy features, such as increased generation of •OH radicals [15], a tuneable band gap [16], improved charge separation [17], and good photocatalysis [6,8,18]. Additionally, the eggshell-derived calcium oxide (CaO) nanoparticles with 1 g/L catalyst loading showed 76% methylene blue (MB) dye degradation under 45-min sunlight exposure [18]. Another study found that approximately 98% of 10 ppm MB could be photodegraded by 12.5 g/L of CaO under 180-min solar irradiation [6]. Furthermore, CaO improved the charge transfer of g-C_3N_4 during crystal violet (CV) dye degradation under visible light illumination [17].

Following another low-cost material, CQD is well-known for its non-toxicity, biocompatibility, great photostability, adjustable optical characteristics, good water dispersity, and excellent light harvesting capabilities [19]. However, the photocatalytic activity of single CQD is weak due to inefficient charge separation and transfer [5]. To increase charge transmission, CQD is functionalised with metal ions. It has been observed that functionalisation can produce oxygen-rich defects on CQD, resulting in improved charge separation of photoinduced electron/hole and charge transfer by trapping photoexcited electrons at surface sites [5]. A study demonstrated that the CQD functionalized onto a polymer, forming a conjugating polyethylene glycol-CQD with calcium ions, could improve the performance [20]. Another study found that CQD operate as an electron reservoir, trapping photoinduced electrons transported from Fe_2O_3 [21], delaying electron-hole charge recombination and enhancing charge transfer for photodegradation.

To date, there is still lack of study that integrating CQD with CaO as a photocatalyst in MB degradation under visible light. This is very crucial to design and synthesize an effective and efficient photocatalyst to remediate the discharge from the textile industry. Hence, in this study, biowaste orange peel-derived CQD is integrated with CaO to improve surface-active sites, charge separation and transfer, fostering an increase in the number of charge carriers for MB photodegradation. The production of valuable advanced materials, CQD/CaO derived from biomass wastes, using a cost-effective, green synthetic technique exemplifies the concept of converting waste to riches. This technique not only helps to manage waste and reduce environmental pollution, but it also promotes

a circular economy and environmental sustainability by repurposing kitchen waste product. Photodegradation of MB to non-harmful compounds such as CO_2 and H_2O has the potential to greatly enhance water quality and human health.

2. Methodology

2.1 Materials

The orange peel waste was obtained from domestic waste in the local kitchen. Ethylene glycol and calcium oxide (CaO) with analytical grade were purchased from Bendosen and used without further purification. All aqueous solutions were prepared with distilled water.

2.2 Procedures

2.2.1 Preparation of biowaste-derived carbon quantum dot (CQD)

The orange peel waste was collected and dried at 150 ° C for 10 h. The dried orange peel waste was cut and ground into tiny pieces of powder form, then sieving to approximately 75 μm. The dried orange peel powder (1 g $\pm$ 2%) was then mixed with ethylene glycol (EG) solution. Next, the mixture solution was sonicated for 30 min to disperse the powder homogeneously in the solution. Subsequently, the sonicated solution was heated at microwave power of 800 W for 60 s. The solution was left for a while to cool to room temperature, followed by centrifugation at 10,000 rpm for 20 min. After 20 min, the solution was separated into two layers – precipitation and supernatant. The precipitation was discarded, and the supernatant was sequentially filtered using 0.45 µm and 0.20 µm syringe filters. The filtered CQD solution was then stored in a fridge for further synthesis and testing. The CQD preparation procedure is illustrated in Figure 1.

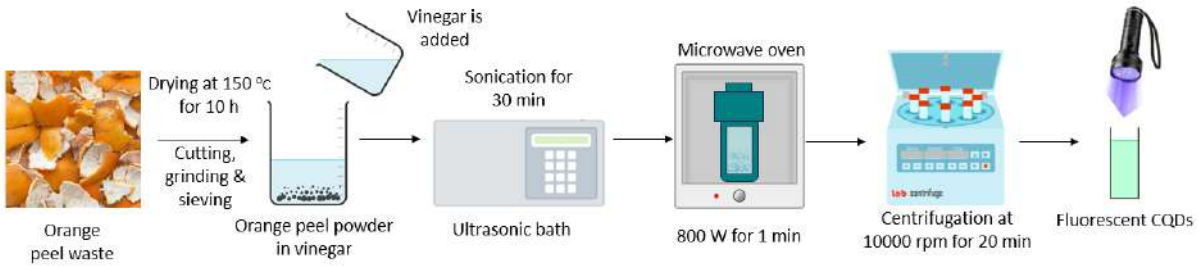

Fig. 1. Synthesis of biomass-derived carbon dots via microwave irradiation

2.2.2 Preparation of CQD/CaO

The CQD/CaO was prepared using hydrothermal treatment. The CaO was added with 20 mL distilled water. This was followed by addition of 10 mL CQD and stirred for 2 hours at room temperature. The mixture solution was then transferred into a 100 mL Teflon-lined stainless-steel autoclave and heated at 180 ° C for 12 h in an oven. After that, the autoclave was cooled down to room temperature and the mixture was centrifuged at 8000 rpm for 10 min. The particles obtained were rinsed and washed with distilled water and ethanol for several times, followed by drying at 80 ° C for 12 h. The schematic diagram of CQD/CaO is depicted in Figure 2.

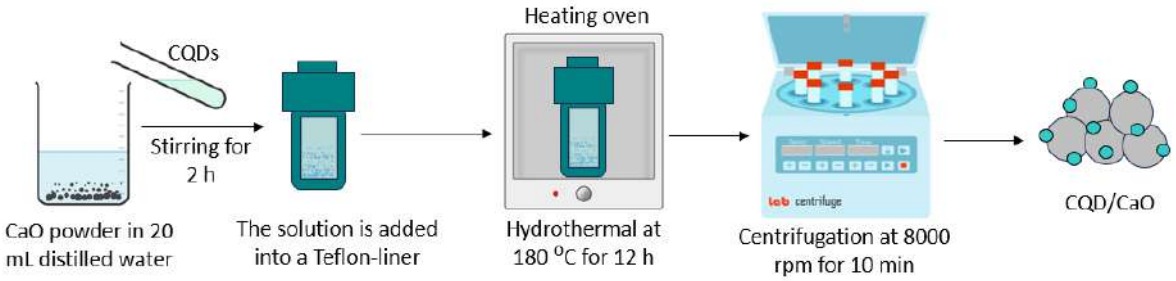

Fig. 2. The synthesis of CQD/CaO using hydrothermal method

2.2.3 Characterizations of the CaO, CQD, and CQD/CaO

The Spectrum One Fourier Transform Infrared Spectroscopy (FTIR, brand: Perkin Elmer) with KBr pellets was used to characterize all of the photocatalyst samples within the range of 400 to 4000 cm^{-1}. The scanning rate was set as 4 cm^{-1}. A mixture of 1:100 catalyst to KBr was prepared and finely crushed into a fine powder under clean conditions. Subsequently, the catalyst/KBr blend was pressed into a thin pallet under 10 ton of pressure using a hydraulic press. The pellet was then loaded into the sample compartment of the FTIR instrument for analysis. Fourier-transform Infrared spectroscopy (FTIR) – to study the surface functional groups of the photocatalysts.

The photocatalysts were characterized by double beam Diffuse Reflectance-Ultraviolet Visible (DR-UV VIS, brand: Shimadzu) with the range of 200 nm to 800 nm. $BaSO_4$ was used as the reference to determine the baseline. Ensure that the powder was evenly dispersed to fully cover the mirror of the sample holder. The DR-UV Vis spectrophotometer was setup with 200 nm/min of scanning speed. A wavelength (x-axis) vs absorbance (y-axis) curve was plotted and Tauc Plot was plotted out using these equations, $E=1240/\lambda$ on the x-axis and $(ahu)^2$ on the y-axis. The n=1/2 was used due to its direct allowed transition. Extrapolation was carried out in the linear region of the plot to the x-axis and the point at which it intersected was determined. The band gap values were then determined from the Tauc plot.

Photoluminescence (PL) emission spectra were measured on a Raman spectrometer at room temperature with the Xenon lamp at the excitation light of 325 nm. The PL spectra in the range of 200 – 600 nm were investigated.

X-ray diffraction (XRD) patterns of the sample was collected on a Bruker D8 Advance diffractometer equipped with a LynxEye detector. Measurements were performed at room temperature using Cu Kα radiation (λ = 1.5418 Å) generated at 40 kV and 40 mA. Data were recorded over a 2θ range of 0 – 80° with a step size of 0.02° and a counting time of 0.3 s per step.

2.2.4 Photodegradation using CQD/CaO under visible-light irradiation

The photodegradation study of the MB was carried out using a 500 mL Pyrex quartz photoreactor equipped with a separable quartz compartment housing the visible light source (300 W Tungsten lamp). The photoreactor covered with aluminum foil was kept under dark environment. Then, CQD/CaO was suspended and stirred in an aqueous solution containing MB for 1 hour for adsorption-desorption equilibrium at dark condition. The adsorption-desorption equilibrium was constructed to prove the pollutant was adsorbed onto the CQD/CaO under dark condition. After that, the photoreactor jacketed with water-cooling circulation was irradiated under 300 W Xenon lamp at ambient temperature. During visible-light illumination, every 3 mL aliquot was taken using syringe at each 20-min interval. The MB degradation was analyzed using UV-vis spectroscopy. The wavelength

of MB appeared at 645 nm. The catalyst loading (0.1, 0.25 and 0.5 g/L) and MB concentration (10, 15, 20 ppm) were examined.

3. Results and Discussion

3.1 The Formation of CQD via Microwave Irradiation Treatment

Photoluminescence under ultraviolet (UV) light serves as a widely utilized and dependable criterion for verifying the effective synthesis of carbon quantum dot (CQD). Figure 3 displays that the CQD solution appeared brown colour under normal day light but displayed a pronounced blue emission when subjected to 365 nm UV light. This fluorescence aligns with the established photoluminescent characteristics of CQD synthesized via hydrothermal carbonization, thereby validating the efficacy of our method in producing luminescent carbon nanomaterials. The distinct UV-induced emission provides direct visual confirmation of the successful synthesis of CQD from biomass precursors. The past study reported that the CQD sourced from banana peels via hydrothermal method exhibited intense blue fluorescence under 365 nm UV irradiation, illustrating the characteristic optical properties of CQD and confirming their effective synthesis [12]. A comparable phenomenon was noted in this investigation as well.

(a) (b)

Fig. 3. CQD under (a) normal light condition and (b) 365 nm UV irradiation

3.2 Physicochemical Properties of CQD/CaO

3.2.1 Photoluminescence (PL) analysis

Figure 4 (a) illustrates the photoluminescence (PL) spectra of CQD under excitation wavelengths of 360 and 420 nm. The observed emission peaks shift from 469 to 514 nm with increasing excitation wavelength, demonstrating excitation-dependent PL behavior. This phenomenon is attributed to the presence of various surface states and size distributions within the CQD, leading to multiple emissive centres [22]. The excitation-dependent emission is a distinctive attribute of CQD, resulting from their unique electronic structures and surface properties. This feature increases their utility in photocatalysis by facilitating wider light absorption and enhancing charge carrier dynamics [23]. The adjustable photoluminescent features of CQD can be utilized to enhance their interaction with other semiconductor materials, hence aiding in the creation of effective heterojunctions for photocatalytic applications [24]. Figure 4 (b) displays the PL spectra of the CQD/CaO nanocomposite under excitation wavelengths of 360 and 420 nm. Similar to the pristine CQD, the CQD/CaO nanocomposite exhibits an excitation-dependent PL activity. The observed emission peaks transition from 468 to 515 nm as the excitation wavelength increases. In comparison to pristine CQD, the nanocomposite demonstrates markedly decreased PL intensity, signifying inhibited electron-hole recombination. This suppression indicates efficient charge separation enabled by the heterojunction between CQD and CaO, similarly as reported in a study that emphasizes on the synergistic effects of carbon dots-based nanocomposites [25]. The incorporation of CQD with CaO improves the separation and

transfer of photogenerated charge carriers, therefore enhancing the photocatalytic efficacy of the nanocomposite [26]. The incorporation of CQD generates additional energy levels in the band structure of CaO, enhancing visible-light absorption and thus increasing photocatalytic activity [27]. Figure 4 (c) juxtaposes the PL spectra of pristine CQD and the CQD/CaO nanocomposite. The nanocomposite shows a significant reduction in PL intensity compared to pristine CQD, supporting the idea of improved charge separation and diminished recombination rates. This enhancement is vital for photocatalytic applications, as it amplifies the availability of charge carriers for redox processes [28]. The establishment of a heterojunction between CQD and CaO not only promotes charge separation but also broadens the light absorption range of the nanocomposite into the visible spectrum, thus improving its photocatalytic efficacy [29]. Furthermore, the synergistic interaction between CQD and CaO might result in the creation of novel active sites, hence enhancing the photocatalytic destruction of contaminants [30].

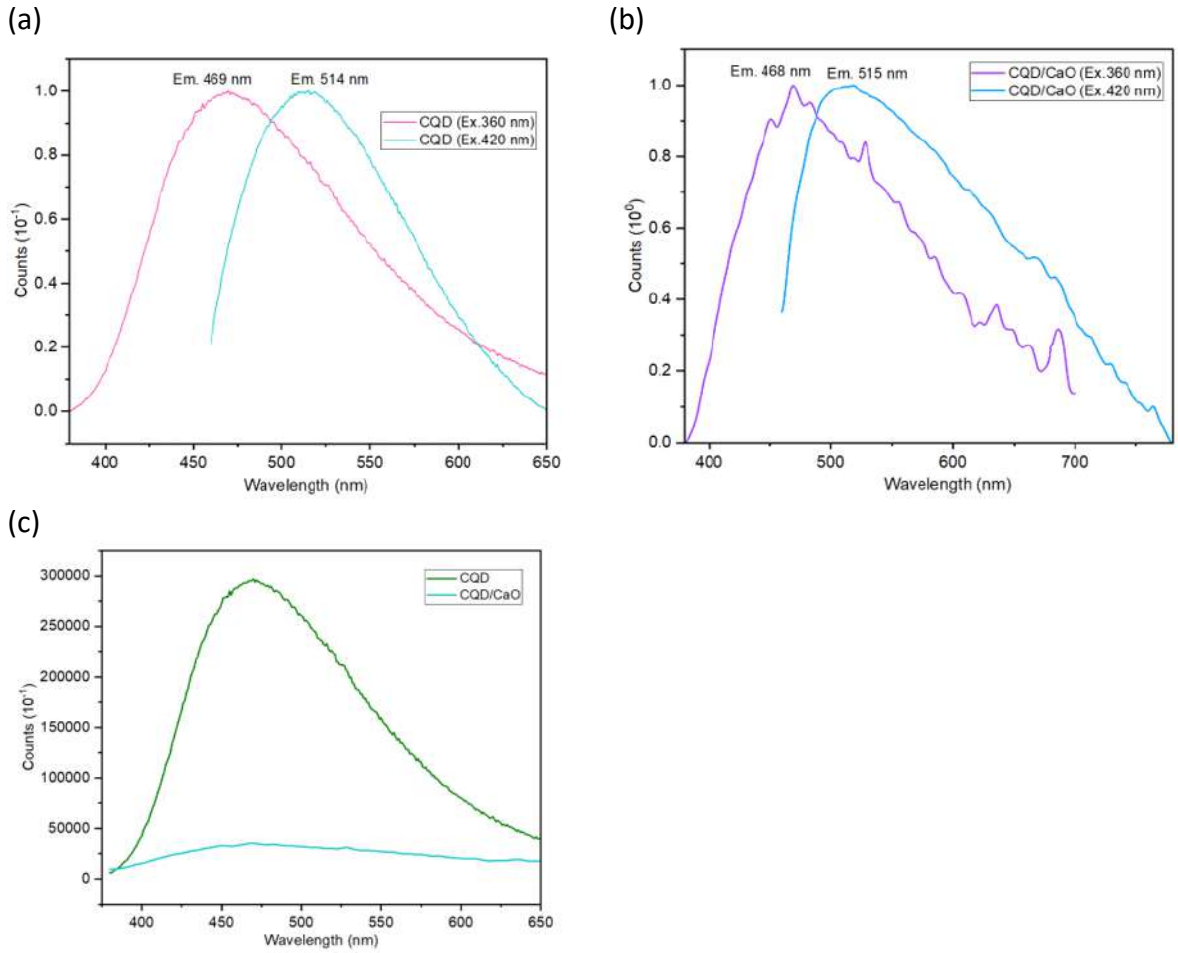

Fig. 4. PL spectra at excitation wavelengths of 360 and 420 nm for (a) CQD and (b) CQD/CaO; (c) PL spectra of CQD and CQD/CaO at excitation wavelength at 420 nm

3.2.2 FTIR analysis

The FTIR study of biowaste-derived CQD and CQD/CaO provides essential insights into the surface chemistry influencing their photocatalytic properties. Figure 5 presents the pristine CQD spectrum with a strong and broad absorption peak at 3295 cm^{-1}, attributed to the stretching vibration of hydroxyl groups (-OH) indicating a high density of hydrophilic functional groups on the CQD surface [31] This hydrophilicity is crucial for promoting dispersion in aqueous environments and facilitating

the adsorption of dye molecules such as cationic methylene blue (MB). Additional peaks observed at 2934 and 2874 cm^{-1} correspond to C-H stretching, while a prominent peak at 1620 cm^{-1} reflects C=C stretching vibrations, confirming the presence of an aromatic carbon framework. C-O stretching vibrations around 1083 and 1033 cm^{-1} further suggest that CQD possess ether and alcohol functionalities, enhancing their water solubility and interaction with pollutants.

After hybridization with CaO, FTIR spectrum of the CQD/CaO nanocomposite exhibits significant changes. A new, sharper -OH stretching peak emerges at 3640 cm^{-1}, attributed to hydroxyl groups introduced by CaO [15]. This indicates that the nanocomposite surface now carries additional active hydroxyl sites, which are known to facilitate the formation of hydroxyl radicals (•OH) under visible-light irradiation, a key intermediate in the degradation of organic pollutants. The C=C stretching band around 1596 cm^{-1} remains evident, confirming that the fundamental electronic structure of the CQD is preserved even after nanocomposite formation, which is critical for maintaining effective light absorption in the visible range. A slight shift in the C-O stretching peak to 1087 cm^{-1} suggests new chemical interactions between CQD and CaO, supporting the formation of chemical bonds that improve charge transfer dynamics and suppress the recombination of photogenerated electron-hole pairs [17].

The increase in hydrophilicity due to the presence of additional surface hydroxyl groups on CQD/CaO is particularly significant. In photocatalysis, enhanced hydrophilicity ensures better dispersion of the photocatalyst in aqueous systems and promotes the adsorption of dye molecules onto the catalyst surface, leading to improved interaction between the active sites and pollutants [32]. In contrast, hydrophobic materials tend to aggregate in water, significantly reducing the number of active sites exposed to pollutants and thereby decreasing photocatalytic efficiency [33]. Hence, the observed shift towards greater hydrophilicity in CQD/CaO nanocomposites is an important factor in their superior photocatalytic performance, directly supporting the degradation efficiency observed during visible-light experiments.

This FTIR characterization directly addresses the research objective of synthesizing a functional CQD/CaO photocatalyst and elucidating how its physicochemical properties influence photocatalytic degradation. The retention of the CQD's aromatic framework ensures strong visible-light absorption, while the enhanced hydrophilic surface facilitates better interaction with aqueous dye pollutants, satisfying the design principle of maximizing charge carrier utilization and pollutant contact. Through effective surface engineering as evidenced by FTIR, the study demonstrates how material modification can optimize photocatalytic activity for environmental remediation purposes. These findings are consistent with previous studies, which showed that increased surface hydroxylation on carbon-based photocatalysts improves pollutant degradation rates by promoting better charge separation and radical formation [31]. Furthermore, the interaction between CQD and CaO introduces heterojunction interfaces that enhance charge transfer while simultaneously improving hydrophilicity [32].

The FTIR data demonstrate that CQD/CaO nanocomposites exhibit optimal surface chemistry, marked by robust hydrophilic functionalities and preserved electronic conjugation, essential for improving photodegradation efficacy under visible light. The capability to create hydrophilic surfaces with active chemical bonds among components exemplifies an effective approach for developing high-efficiency photocatalysts for wastewater treatment, furthering the overarching objective of sustainable and eco-friendly environmental solutions.

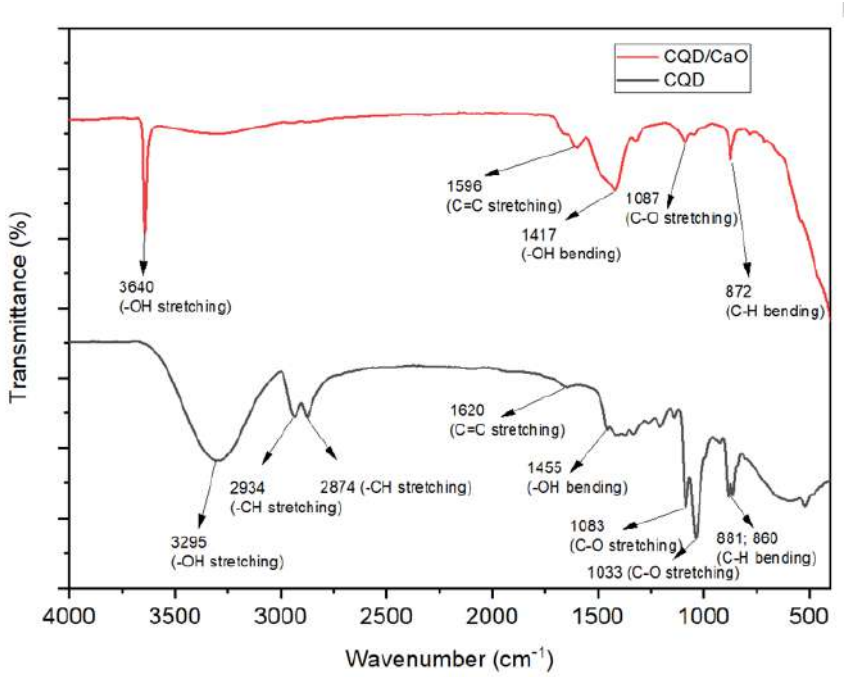

Fig. 5. FTIR spectra of as-synthesized CQD and CQD/CaO nanocomposite

3.2.3 UV-VIS analysis

Figure 6 (a) illustrates the UV-Vis examination of biowaste-derived CQD, offering critical insights into their optical characteristics and photocatalytic capabilities. The absorption spectra reveal a prominent peak at around 280 nm, commonly linked to $\pi \rightarrow \pi^*$ transitions of aromatic sp^2 regions within the carbon framework [31]. This signifies that CQD possess a substantial conjugated system, an essential characteristic for improving electron mobility and light absorption. Additionally, a wide absorption shoulder extending into the visible spectrum is apparent, indicating the existence of $n \rightarrow \pi^*$ transitions associated with surface functional groups like C=O and -OH [32]. These characteristics indicate a beneficial framework for photocatalytic applications; wherein effective light absorption is essential for the generation of active charge carriers. The optical band gap of the CQD, as determined from the Tauc plot, is around 3.09 eV. This relatively wide band gap places the CQD primarily within the UV light absorption range, yet the observed visible-light tail hints at their capacity to respond under lower-energy illumination. Furthermore, the good optical absorption behavior supports the CQD's role in improving charge carrier generation and separation. The enhanced light harvesting across UV and partial visible spectra ensures that a larger number of photogenerated electrons and holes are available for redox reactions. Compared to other carbon-based materials, CQD show favorable characteristics similar to previously reported biomass-derived quantum dots, which have demonstrated excellent performance in photocatalytic dye degradation [31]. Their comparatively broad band gap indicates a high redox potential, an advantageous characteristic for facilitating oxidation and reduction reactions essential in wastewater treatment applications [34].

Figure 6 (b) presents the UV-Vis absorption spectra of the CQD/CaO nanocomposite, which conveys critical insights into its optical and electrical characteristics pertinent to photocatalytic applications. In comparison to pure CQD, the absorption spectrum of CQD/CaO is expanded and reaches into the visible light spectrum, signifying improved light harvesting efficiency. The optical band gap of CaO is between 3.60 eV [35] and 3.90 eV [18], the as-synthesized CQD is around 3.09 eV, and the CQD/CaO nanocomposite is roughly 2.92 eV. This reduction in CQD/CaO band gap compared to pristine CQD and CaO, suggesting that this heterojunction effectively narrows the energy

separation between the valence and conduction bands, facilitating more efficient charge separation and transfer [34]. A slightly smaller band gap enables the CQD/CaO nanocomposite to utilize a broader portion of the solar spectrum, thereby generating more photogenerated electron-hole pairs during illumination [32]. Moreover, the presence of CQD, with their excellent electron transfer capabilities, aids in the improved separation of photoexcited charge carriers. This synergistic effect between CQD and CaO leads to the suppression of electron-hole recombination, a major limitation in many wide-bandgap semiconductor systems, thus enhancing photocatalytic efficiency [17].

The absorption profile also shows that CQD/CaO nanocomposite has introduced additional intermediate energy levels within the band structure, likely due to the interaction between surface oxygen-containing functional groups of CQD. The broadening into the visible range is largely attributed to surface defect states and oxygen-containing groups, which create localized energy levels within the band structure, enabling sub-bandgap excitation. These mid-gap states facilitate photon absorption at lower energies, contributing to the visible-light activity. Such modification of electronic structure through heterojunction formation is well-documented as a strategy to boost photocatalytic activity by promoting efficient charge migration across interfaces [32]. Compared to standalone CaO, which typically suffers from poor light absorption and rapid recombination, the integration with CQD clearly improves both optical properties and charge dynamics [17]. Coupling CQD with CaO creates a complementary band alignment that facilitates efficient interfacial charge transfer. This synergy suppresses electron-hole recombination, thereby significantly enhancing the overall photocatalytic performance [32]. This proves that fabricating a hybrid photocatalyst that overcomes the intrinsic limitations of individual components by leveraging the complementary advantages of CQD's light-harvesting ability and CaO's chemical stability.

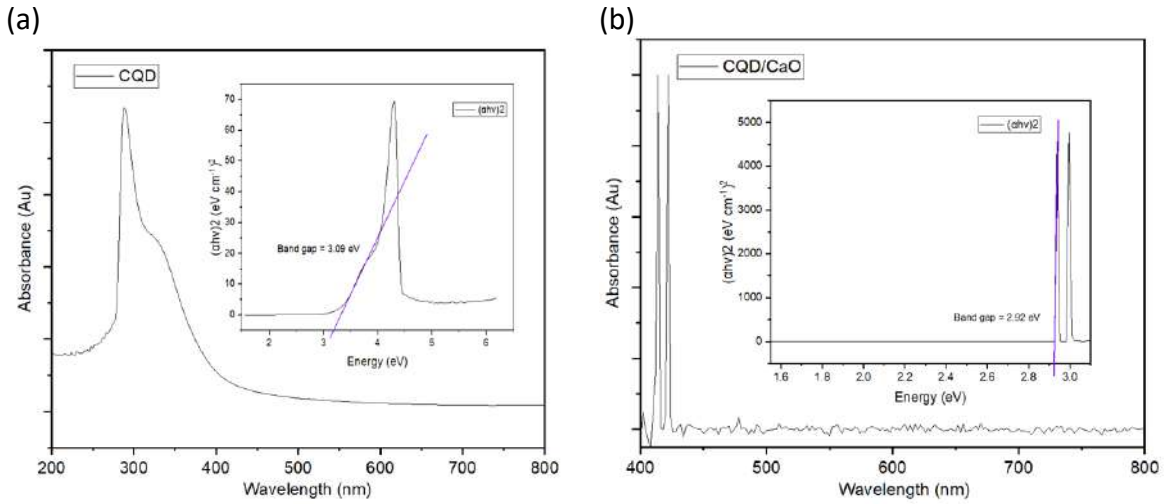

Fig. 6. (a) UV-Vis absorption spectrum and Tauc plot analysis of CQD; (b) UV-Vis absorption spectrum and Tauc plot analysis of CQD/CaO

Overall, the UV-Vis analysis confirms that the CQD/CaO nanocomposite has achieved the targeted band structure engineering for visible-light photocatalysis. The enhanced absorption and narrower band gap ensure a higher probability of photogenerated charge carriers participating in redox reactions, crucial for the photodegradation of organic pollutants. These findings provide strong support that the microwave-hydrothermal synthesis method successfully produced a functional material with improved photocatalytic properties.

3.2.4 XRD analysis

The X-ray diffraction (XRD) pattern of the synthesized CQD/CaO nanocomposite is presented in Figure 7. The diffractogram demonstrates a hybrid structural nature, characterized by both a broad amorphous band and a series of sharp crystalline peaks. The broad band centered in the 2θ range of 15°–25° is attributed to the amorphous CQD incorporated within the nanocomposite. This signature feature is consistent with prior studies of CQD, where the lack of long-range order in carbon-based nanostructures results in a wide, low-intensity diffraction region. It is reported a similar broad amorphous region for CQD synthesized from biowaste, confirming the non-crystalline nature of these carbon domains [13,14]. Superimposed on this broad band are a number of sharp peaks at 2θ values of approximately 24.9°, 27.7°, 29.3°, 32.1°, 39.3°, 43.7°, 49.7°, and 55.8°. These peaks are indexed to the (111), (200), (220), (311), and other characteristic lattice planes of crystalline calcium oxide (CaO), matching well with the reference pattern (JCPDS No. 37-1497). Notably, the most intense peak at 2θ ≈ 29.3° corresponds to the (200) plane of CaO, indicating the presence of highly crystalline CaO in the composite. Such observations that the crystalline phases in CaO-based composites are readily identified by their sharp, well-defined XRD reflections, confirming the purity and crystallinity of the CaO structure are supported by literatures [6,18].

The absence of additional impurity peaks or secondary phases further corroborates the successful integration of CQD and CaO, indicating that the synthetic process did not introduce unwanted byproducts. This purity is crucial for photocatalytic applications, as impurities often serve as recombination centers, negatively affecting the separation and mobility of charge carriers. The coexistence of amorphous CQD and crystalline CaO creates a heterojunction structure that is highly advantageous for photocatalysis. Amorphous CQD provide a rich population of defect sites and surface functional groups, which facilitate the trapping and transfer of photogenerated charge carriers. Meanwhile, the highly crystalline CaO offers abundant catalytic sites and structural stability, further enhancing photocatalytic activity. The XRD analysis confirms the formation of a composite with both amorphous and crystalline components, a structure well-documented to be beneficial for visible-light-driven photocatalytic applications.

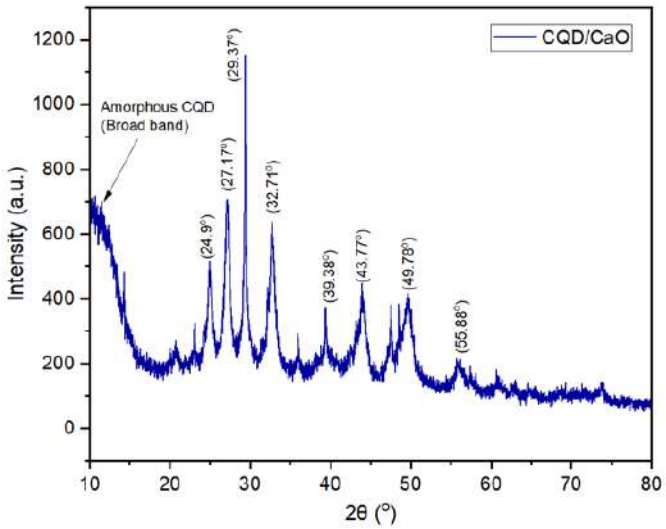

Fig. 7. X-Ray Diffraction result of CQD/CaO nanocomposite

3.3 Methylene Blue (MB) Photodegradation
3.3.1 MB initial concentration

Figure 8 illustrates the photodegradation profiles of MB at three different initial concentrations (10, 15, and 20 ppm) over a duration of 180 min under visible-light irradiation using the CQD/CaO photocatalyst. The 15 ppm MB solution exhibits the highest degradation, rising sharply after 60 min and reaching approximately 72% at 180 min, significantly surpassing the performances of both the 10 ppm and 20 ppm solutions. In comparison, 20 ppm solution exhibits a more gradual increase in degradation, only achieving around 52% at the end of the 180-min period. This slower rate could be attributed to the increased optical density at higher MB concentration, leading to reduced photon penetration. Conversely, 10 ppm MB solution shows an intermediate trend, ultimately achieving about 54% degradation efficiency. This lower initial concentration might limit interactions between the MB molecules and the active catalytic sites, thus limiting the efficiency. This comparative analysis highlights that 15 ppm concentration represents an optimal balance, maximizing the effective utilization of both photons and active catalytic sites, thereby achieving the highest photodegradation performance.

Firstly, at higher concentrations such as 20 ppm, the solution contains a larger number of MB molecules per unit volume. This high pollutant loading leads to the increased occupation of active sites on the photocatalyst surface, resulting in a phenomenon known as surface saturation [36]. Once these sites are saturated, additional dye molecules cannot be efficiently adsorbed and degraded, which limits the overall degradation efficiency. Moreover, excessive MB molecules can act as optical filters, absorbing incident light and reducing the number of photons reaching the catalyst surface, thus decreasing the generation of reactive species such as hydroxyl radicals (•OH). As a result, the photodegradation efficiency is lower despite the presence of sufficient photocatalyst [36]. On the other hand, at very low concentrations such as 10 ppm, although there is no significant surface saturation, the absolute number of MB molecules available for degradation is limited. This leads to a scenario where the production of reactive oxygen species (ROS) by the photocatalyst is underutilized[37]. In other words, the rate of photogenerated charge carrier consumption is lower because there are fewer dye molecules to react with. Consequently, while the degradation per molecule may be fast, the overall observed degradation percentage appears smaller compared to the optimal condition. The solution with 15 ppm concentration represents a balanced condition where the number of MB molecules is sufficient to maximize interaction with available active sites without causing surface saturation. Additionally, the dye concentration is not high enough to induce significant light scattering or shielding effects. Therefore, the photons can efficiently reach the catalyst surface, ensuring robust production of ROS, while the MB molecules present in the solution can rapidly react with the active species [38]. This synergy between efficient photon absorption, active site availability, and adequate pollutant load leads to the highest degradation efficiency observed at 15 ppm.

Another important factor is the recombination rate of photogenerated electrons and holes. At excessively high pollutant concentrations, the recombination of charge carriers tends to increase because the accumulation of pollutant molecules near the catalyst surface hampers the migration and separation of charges [36,38]. Meanwhile, at very low concentrations, charge carriers may recombine without participating in pollutant degradation due to the scarcity of reactant molecules [37]. Therefore, an intermediate concentration like 15 ppm allows for optimal charge utilization, where most of the generated electrons and holes are effectively consumed in the degradation reactions rather than undergoing recombination.

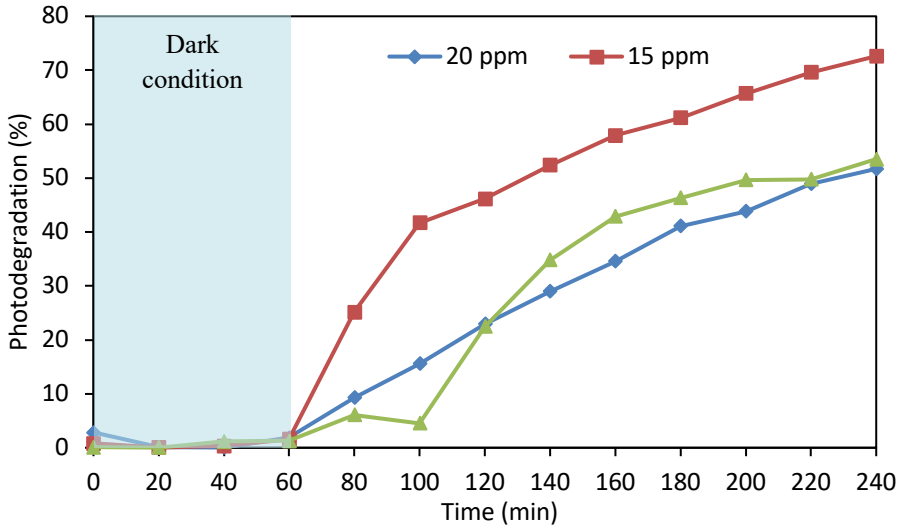

Fig. 8. A comparison of the efficiency of MB photodegradation at three concentrations of MB (10 ppm, 15 ppm, and 20 ppm)

In summary, the superior degradation performance at 15 ppm MB concentration can be attributed to a combination of optimized surface adsorption, efficient light utilization, balanced ROS generation, and minimized electron-hole recombination. These factors collectively enable the CQD/CaO photocatalyst to exhibit its highest photocatalytic activity under these conditions. The observed trend is well supported by existing literature on photocatalysis kinetics and surface science, emphasizing the critical role of pollutant concentration in optimizing photocatalytic degradation performance [36-38].

3.3.2 Catalyst loading

Figure 9 shows the photocatalytic degradation results of MB at different CQD/CaO catalyst dosages (0.1 g/L, 0.25 g/L, and 0.5 g/L) reveal that the 0.25 g/L condition achieves the highest photodegradation efficiency, reaching approximately 72.6% after 180-min visible-light irradiation. This trend can be explained by analyzing the interplay between catalyst surface area, light penetration, and charge carrier dynamics.

At a low catalyst loading of 0.1 g/L, the available active surface area is limited, resulting in fewer sites for photon absorption and reactive species generation [39]. Although the solution remains optically transparent, the insufficient quantity of photocatalyst restricts the number of photogenerated electrons and holes, leading to a slower degradation rate and lower overall removal efficiency. Previous studies have shown that when the catalyst amount is too low, the generation of reactive oxygen species (ROS) becomes insufficient to drive efficient degradation reactions [39]. Conversely, when the catalyst dosage is increased to 0.5 g/L, a decline in photodegradation efficiency is observed compared to the 0.25 g/L optimal dosage. Excessive photocatalyst loading leads to light scattering and reduced light penetration into the reaction mixture [40]. As the suspended particles become denser, they block and scatter incoming photons, preventing effective activation of the photocatalyst deeper inside the solution. Moreover, high catalyst concentrations can promote particle agglomeration, reducing the effective surface area accessible to reactants [40]. The catalyst dosage of 0.25 g/L appears to strike an optimal balance between sufficient active sites and effective photon absorption. At this concentration, the CQD/CaO nanocomposite generates a high density of charge carriers while maintaining good light penetration and dispersion in the solution [41].

Furthermore, the recombination rate of photogenerated electron-hole pairs is minimized under these conditions because the ROS generated are quickly consumed by available dye molecules, enhancing photocatalytic efficiency [41]. In this ideal region, both mass transfer and reaction kinetics are advantageous, resulting in the highest recorded photodegradation rate.

The 0.25 g/L catalyst loading achieves an optimal equilibrium of adequate surface-active sites, effective light consumption, and minimal recombination losses, yielding superior photodegradation performance. Both insufficient and excessive catalyst dosages result in suboptimal conditions—either from restricted active sites or excessive light scattering—underscoring the imperative to optimize catalyst quantities in photocatalytic systems [39-41].

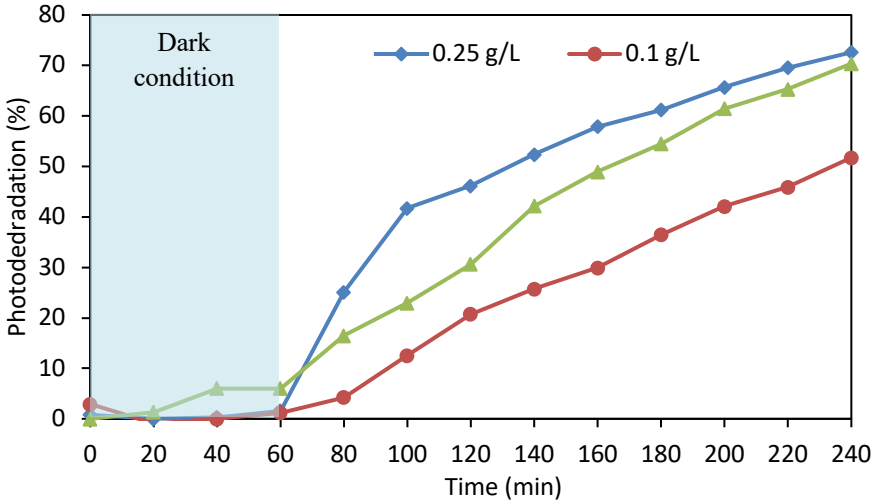

Fig. 9. A comparison of the efficiency of MB photodegradation at three catalyst loadings (0.1 g/L, 0.25 g/L, 0.5 g/L)

3.3.3 Kinetic analysis

Figure 10 (a) shows the first-order kinetic plots for MB photodegradation at different initial concentrations (10, 15, and 20 ppm) using catalyst loading of 0.5 g/L. It is evident that the degradation rate constant (k) decreases as the initial MB concentration increases: k = 0.0052 min^{-1} (15 ppm) > k = 0.0029 min^{-1} (10 ppm) > k = 0.0027 min^{-1} (20 ppm). This trend is also reflected in the half-life values ($t_1/_2$), with 15 ppm showing the shortest half-life (133.3 min), followed by 10 ppm (231.8 min), and 20 ppm having the longest (256.7 min). These results indicate that a dye concentration of 15 ppm allows for the most efficient photodegradation. At a lower concentration, all dye molecules are accessible to active sites, but overall reaction is slower due to lower reactant availability. At a higher concentration, although more dye molecules are present, they can saturate the catalyst's active sites and cause excess light attenuation (inner filter effect), both of which reduce degradation efficiency. The observed kinetics fit the pseudo-first-order model well (R^2 > 0.93 for all cases), which is typical for heterogeneous photocatalysis. A similar trend has been reported by Senthilkumaar *et al*., [42], who studied the photodegradation of methyl orange (MO) by TiO_2 and found that the apparent rate constant decreased as initial dye concentration increased, due to limited availability of active sites and increased light scattering at higher concentrations. Their results underline the importance of optimizing initial pollutant concentration for efficient photocatalytic treatment. According to Langmuir–Hinshelwood (L–H) kinetics, which often describe heterogeneous photocatalysis, the apparent reaction rate first increases with concentration but eventually levels off or declines at high concentrations due to saturation effects [37]. The L–H model supports the experimental data, suggesting that 15 ppm falls within the concentration range where the

degradation rate is near its maximum before adverse effects such as light attenuation and site blocking become dominant.

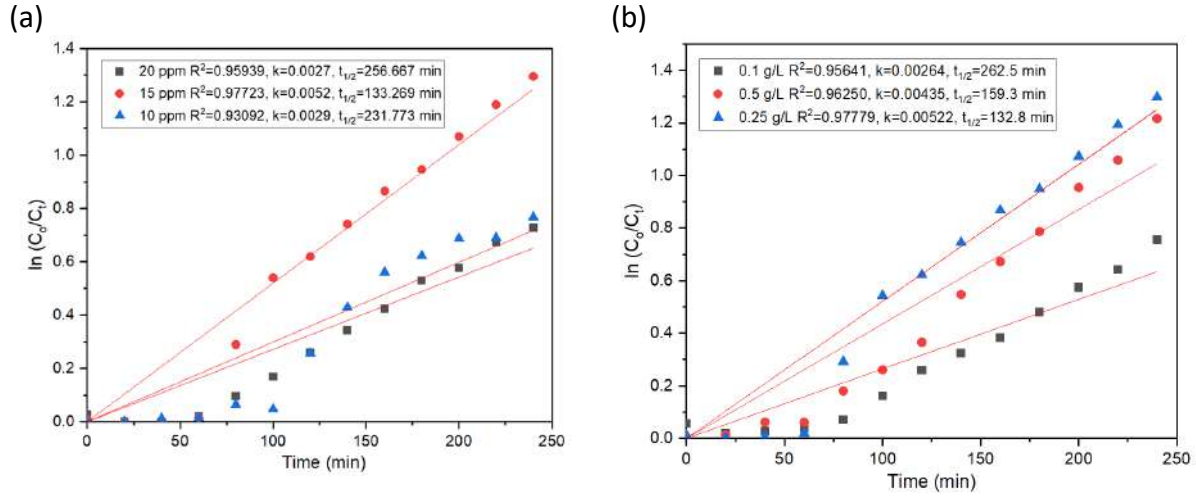

Fig. 10. (a) Pseudo-first-order kinetic plots for MB photodegradation using (a) 0.5 g/L catalyst loading at initial pollutant concentrations of 10, 15, and 20 ppm; (b) 15 ppm initial pollutant concentration at catalyst loadings of 0.1, 0.25, and 0.5 g/L

Figure 10 (b) presents first-order kinetic plots for MB photodegradation at a constant initial dye concentration (15 ppm) but varying catalyst dosages (0.1, 0.25, and 0.5 g/L). The results demonstrate that increasing the catalyst loading significantly enhances the degradation. The highest rate constant ($k = 0.00522\ min^{-1}$) and shortest half-life ($t_1/_2 = 132.8$ min) are observed at 0.25 g/L, while the lowest k value ($0.00264\ min^{-1}$) and longest half-life (262.5 min) are observed at 0.1 g/L. The enhancement in degradation rate with increasing catalyst dosage is attributed to the greater availability of active sites for photon absorption and dye adsorption, which in turn increases the generation of reactive species such as hydroxyl radicals. However, the catalyst loading of 0.5 g/L ($k = 0.00435\ min^{-1}$), beyond an optimal point, further increases in catalyst concentration can lead to particle aggregation and increased opacity, causing light scattering and reduced effective light penetration. This behavior is consistent with the findings of Yusuff *et al*., [43], who reported that increasing catalyst loading improved the photodegradation rate of MB up to an optimum, beyond which the rate plateaued or even declined due to light shielding and particle crowding. Their work reinforces the importance of balancing catalyst loading to achieve maximal photocatalytic activity without adverse effects from excess catalyst [43]. The observed trend aligns with the Langmuir–Hinshelwood (L-H) kinetic model, which posits that the photocatalytic reaction rate escalates with catalyst concentration until reaching a peak, beyond which additional increases may result in a decrease due to mass transfer limitations and light shielding effects [39]. The experimental results indicate that a dose of 0.25 g/L of CQD/CaO catalyst is optimal for the efficient visible-light-driven degradation of MB.

3.3.4 Proposed heterojunction of CQD/CaO

Figure 11 illustrates the photocatalytic mechanism of CQD/CaO nanocomposites under visible light can be explained based on the formation of a Type-II heterojunction structure between CQD and CaO. A similar system such as Fe_2O_3/CQD composites have been reported to form Type-II band alignments, which enhance light absorption and inhibit charge recombination. The hybrid heterostructure improved charge transfer at the interface and showed higher photocatalytic efficiency compared to pristine hematite or CQD alone [44]. By analogy, the CQD/CaO structure

developed in this work is proposed to exhibit a comparable mechanism, as confirmed by band alignment analysis and PL quenching.

The band structure alignment of CQD/CaO enables effective charge carrier separation and facilitates the generation of reactive oxygen species (ROS), which are essential for the photodegradation of organic pollutants. In a Type-II heterojunction system, the conduction band (CB) of CQD lies higher (i.e., more negative) than that of CaO, while the valence band (VB) of CQD lies lower (i.e., less positive) than that of CaO. Upon light irradiation ($h\nu > Eg$), both CQD and CaO generate electron-hole pairs. The photogenerated electrons (e^-) in CQD migrate to the CB of CaO, while the photogenerated holes (h^+) in CaO transfer to the VB of CQD. This spatial separation of electrons and holes across the interface significantly reduces charge recombination, increasing the lifetime of the charge carriers and enhancing photocatalytic performance [45]. The generation of ROS, including •OH and $\bullet O_2^-$ radicals, is promoted by this efficient charge separation. The transferred electrons on CaO can reduce O_2 molecules to form superoxide radicals ($\bullet O_2^-$), while the holes remaining on CQD oxidize water molecules or OH^- to produce hydroxyl radicals (•OH). The hydroxyl radicals (•OH) play a dominant role in dye degradation, and CQD enhance their formation through secondary ROS pathways [46]. The combination of •OH and singlet oxygen ($^1O_2$) results in a synergistic effect that leads to complete mineralization of pollutants.

A schematic representation of the proposed mechanism is illustrated in Figure 11, which shows how the internal electric field at the heterojunction interface facilitates directional movement of charge carriers, enabling continuous production of ROS under visible light irradiation. The enhanced activity of the CQD/CaO nanocomposite is therefore directly attributed to its Type-II heterojunction architecture.

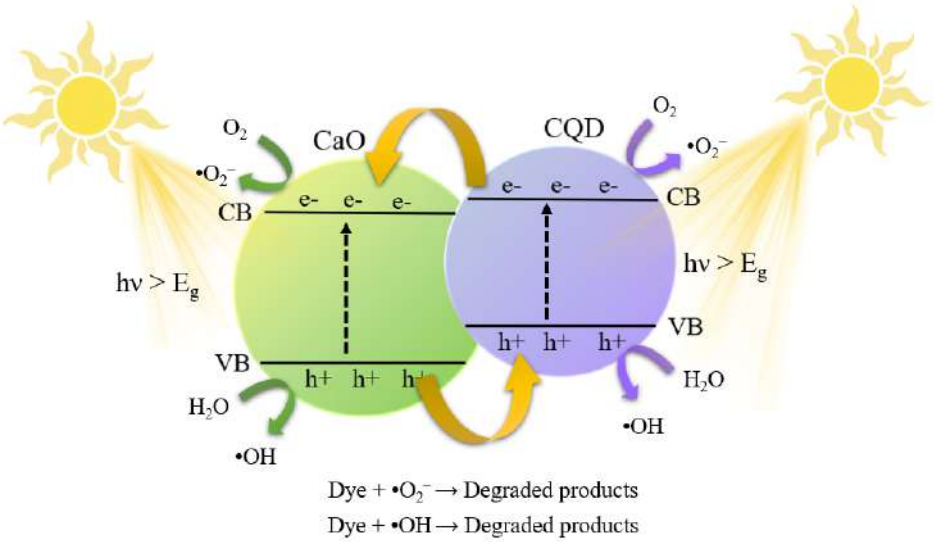

Fig. 11. Proposed type-II heterojunction of CQD/CaO photocatalytic system

4. Conclusions

This study demonstrates the successful engineering of a biowaste-derived carbon quantum dot/calcium oxide (CQD/CaO) nanocomposite and its effective application in the photodegradation of methylene blue (MB) under visible light. The comprehensive characterizations, including FTIR, photoluminescence (PL), UV-Vis spectroscopy, and X-ray diffraction (XRD), clearly reveal the advantageous physicochemical features introduced by the heterojunction structure. FTIR analysis confirmed the presence of abundant hydroxyl and other oxygen-containing functional groups on the CQD surface and their further enrichment after hybridization with CaO. These hydrophilic

functionalities are crucial for enhancing catalyst dispersion in aqueous environments and promoting dye molecule adsorption, both of which are vital for efficient photocatalysis. PL spectra provided strong evidence of improved charge separation in the CQD/CaO nanocomposite, as demonstrated by the pronounced decrease in PL intensity compared to pure CQD. This reduction in electron-hole recombination directly translates to a greater number of available charge carriers participating in redox reactions, a key requirement for high photocatalytic activity. UV-Vis spectroscopy results showed that the CQD/CaO nanocomposite possesses a narrowed band gap (2.92 eV) relative to pristine CQD (3.09 eV), resulting in broader and stronger absorption in the visible-light region. This band structure engineering is pivotal for utilizing solar energy more effectively, enabling the photocatalyst to generate more electron-hole pairs under visible light irradiation. XRD analysis verified the hybrid nature of the nanocomposite, displaying both amorphous CQD domains and highly crystalline CaO, confirming the successful formation of a functional heterojunction without unwanted impurities. Under the optimal reaction conditions, catalyst loading of 0.25 g/L, initial MB concentration of 15 ppm, at pH 7, and with the addition of 10 mL 5 mM H_2O_2, the CQD/CaO nanocomposite achieved a maximum photodegradation efficiency of 72.61% within 180 min of visible light exposure. Kinetic analysis further demonstrated that these conditions promoted the fastest degradation rates. Crucially, the CQD/CaO heterojunction enhances reaction efficiency by providing efficient charge separation pathways, facilitating visible-light absorption, and introducing additional surface-active sites. The synergy between amorphous CQD and crystalline CaO not only suppresses electron-hole recombination but also increases radical generation (•OH), leading to superior photodegradation performance compared to individual components. This research highlights the promise of biowaste-derived CQD/CaO as a sustainable and highly efficient photocatalyst for textile dye removal. The findings offer valuable insights for the rational design of next-generation photocatalysts and contribute to environmental remediation and the advancement of circular economy practices.

Acknowledgement
The work was funded by a grant from Xiamen University Malaysia Research Fund (XMUMRF/2025-C15/IENG/0077).

References

[1] Adaikalam, Kathalingam, Sajjad Hussain, Periasamy Anbu, Arulmozhi Rajaram, Iyyakkannu Sivanesan, and Hyun-Seok Kim. "Eco-friendly facile conversion of waste eggshells into CaO nanoparticles for environmental applications." *Nanomaterials* 14, no. 20 (2024): 1620. https://doi.org/10.3390/nano14201620

[2] Ang, Wei Lun, Cheldclos AL Boon Mee, Nonni Soraya Sambudi, Abdul Wahab Mohammad, Choe Peng Leo, Ebrahim Mahmoudi, Muneer Ba-Abbad, and Abdelbaki Benamor. "Microwave-assisted conversion of palm kernel shell biomass waste to photoluminescent carbon dots." *Scientific Reports* 10, no. 1 (2020): 21199. https://doi.org/10.1038/s41598-020-78322-1

[3] Araújo, Tiago Cabral, Henrique dos S. Oliveira, José Joaquim Sá Teles, Jose Domingos Fabris, Luiz CA Oliveira, and João Paulo de Mesquita. "Hybrid heterostructures based on hematite and highly hydrophilic carbon dots with photocatalytic activity." *Applied Catalysis B: Environmental* 182 (2016): 204-212. https://doi.org/10.1016/j.apcatb.2015.09.036

[4] Atchudan, Raji, Thomas Nesakumar Jebakumar Immanuel Edison, Suguna Perumal, Nallal Muthuchamy, and Yong Rok Lee. "Hydrophilic nitrogen-doped carbon dots from biowaste using dwarf banana peel for environmental and biological applications." *Fuel* 275 (2020): 117821. https://doi.org/10.1016/j.fuel.2020.117821

[5] Bolorizadeh, Mohammad A., V. A. Sashin, A. S. Kheifets, and M. J. Ford. "Electronic band structure of calcium oxide." *Journal of electron spectroscopy and related phenomena* 141, no. 1 (2004): 27-38. https://doi.org/10.1016/j.elspec.2004.04.004

[6] Byrne, J. Anthony, Pilar A. Fernandez-Ibanez, Patrick SM Dunlop, Dheaya MA Alrousan, and Jeremy WJ Hamilton. "Photocatalytic enhancement for solar disinfection of water: a review." *International Journal of Photoenergy* 2011, no. 1 (2011): 798051. https://doi.org/10.1155/2011/798051

[7] Caldas, A. M., D. F. Dos Santos, M. A. M. Castro, M. D. Teodoro, F. V. Motta, and M. R. D. Bomio. "Fabrication of CN-HAp heterostructures from eggshells with improved photocatalytic performance in degrading of mixing dyes under sunlight." *Materials Science in Semiconductor Processing* 165 (2023): 107660. https://doi.org/10.1016/j.mssp.2023.107660

[8] Chandra, Soumen, Angshuman Ray Chowdhuri, Triveni Kumar Mahto, and Sumanta Kumar Sahu. "Nanostructured Fe3O4@ Fe2O3/carbon dots heterojunction for efficient photocatalyst under visible light." *Journal of Nanoscience and Nanotechnology* 17, no. 2 (2017): 1116-1124. https://doi.org/10.1166/jnn.2017.12580

[9] Chen, Peng, Yumeng Liang, Yifeng Xu, Yunliang Zhao, and Shaoxian Song. "Synchronous photosensitized degradation of methyl orange and methylene blue in water by visible-light irradiation." *Journal of Molecular Liquids* 334 (2021): 116159. https://doi.org/10.1016/j.molliq.2021.116159

[10] Chong, Meng Nan, Bo Jin, Christopher WK Chow, and Chris Saint. "Recent developments in photocatalytic water treatment technology: a review." *Water research* 44, no. 10 (2010): 2997-3027. https://doi.org/10.1016/j.watres.2010.02.039

[11] Daneshvar, Nezamaddin, Darioush Salari, and A. R. Khataee. "Photocatalytic degradation of azo dye acid red 14 in water on ZnO as an alternative catalyst to TiO2." *Journal of photochemistry and photobiology A: chemistry* 162, no. 2-3 (2004): 317-322. https://doi.org/10.1016/S1010-6030(03)00378-2

[12] Elugoke, Saheed E., Gloria E. Uwaya, Taiwo W. Quadri, and Eno E. Ebenso. "Carbon quantum dots: basics, properties, and fundamentals." In *Carbon dots: recent developments and future perspectives*, pp. 3-42. American Chemical Society, 2024. https://doi.org/10.1021/bk-2024-1465.ch001

[13] Farhana, Kaniz, Abu Shadate Faisal Mahamude, and Mushfika Tasnim Mica. "The scenario of textile industry in Malaysia: A review for potentiality." *Materials Circular Economy* 4, no. 1 (2022): 20. https://doi.org/10.1007/s42824-022-00063-5

[14] Ghiasi, Maryam, Mahsa Ghanbarzadeh, Ali Ghaffarinejad, and Faezeh Shahdost-Fard. "Green nitrogen and sulfur co-doped carbon dots derived from eggshell as a high performance aptasensing interface for non-invasive detection of metronidazole." *Talanta* 285 (2025): 127363. https://doi.org/10.1016/j.talanta.2024.127363

[15] Gogoi, Jahnabi, and Devasish Chowdhury. "Calcium-modified carbon dots derived from polyethylene glycol: fluorescence-based detection of Trifluralin herbicide." *Journal of Materials Science* 55, no. 25 (2020): 11597-11608. https://doi.org/10.1007/s10853-020-04839-5

[16] Gudimella, Krishna Kanthi, Tejaswini Appidi, Hui-Fen Wu, Venkateswararao Battula, Anil Jogdand, Aravind Kumar Rengan, and Gangaraju Gedda. "Sand bath assisted green synthesis of carbon dots from citrus fruit peels for free radical scavenging and cell imaging." *Colloids and Surfaces B: Biointerfaces* 197 (2021): 111362. https://doi.org/10.1016/j.colsurfb.2020.111362

[17] Han, Wenyuan, Hao Zhang, Degang Li, Wenwu Qin, Xuliang Zhang, Shaobin Wang, and Xiaoguang Duan. "Surface engineered carbon quantum dots for efficient photocatalytic hydrogen peroxide production." *Applied Catalysis B: Environment and Energy* 350 (2024): 123918. https://doi.org/10.1016/j.apcatb.2024.123918

[18] Heng, Zeng Wei, Woon Chan Chong, Yean Ling Pang, Lan Ching Sim, and Chai Hoon Koo. "Photocatalytic degradation of organic pollutants using green oil palm frond-derived carbon quantum dots/titanium dioxide as multifunctional photocatalysts under visible light radiation." *Chinese Journal of Chemical Engineering* 51 (2022): 21-34. https://doi.org/10.1016/j.cjche.2021.10.021

[19] Hu, Xuetao, Yanxiao Li, Yiwei Xu, Ziyu Gan, Xiaobo Zou, Jiyong Shi, Xiaowei Huang, Zhihua Li, and Yahui Li. "Green one-step synthesis of carbon quantum dots from orange peel for fluorescent detection of Escherichia coli in milk." *Food Chemistry* 339 (2021): 127775. https://doi.org/10.1016/j.foodchem.2020.127775

[20] Jaiswal, Krishna Kumar, Swapnamoy Dutta, Cheryl Bernice Pohrmen, Ravikant Verma, Arvind Kumar, and Arun Prasath Ramaswamy. "Bio-waste chicken eggshell-derived calcium oxide for photocatalytic application in methylene blue dye degradation under natural sunlight irradiation." *Inorganic and Nano-Metal Chemistry* 51, no. 7 (2021): 995-1004. https://doi.org/10.1080/24701556.2020.1813769

[21] Jiang, P., C. Liu, C. Yang, L. Y. Zhang, J. W. Liang, and Z. H. Yang. "Study on acoustic emission parameter fusion-based NOL ring damage assessment method for modeling hydrogen storage cylinder shells." *International Journal of Hydrogen Energy* 136 (2025): 1274-1281. https://doi.org/10.1016/j.ijhydene.2024.01.005

[22] Jung, Hwapyung, Vijay S. Sapner, Arindam Adhikari, Bhaskar R. Sathe, and Rajkumar Patel. "Recent progress on carbon quantum dots based photocatalysis." *Frontiers in Chemistry* 10 (2022): 881495. https://doi.org/10.3389/fchem.2022.881495

[23] Ke, Yaotang, Bhaskar Garg, and Yong-Chien Ling. "Waste chicken eggshell as low-cost precursor for efficient synthesis of nitrogen-doped fluorescent carbon nanodots and their multi-functional applications." *RSC advances* 4, no. 102 (2014): 58329-58336. https://doi.org/10.1039/C4RA10178B

[24] Kumar, S. Girish, and L. Gomathi Devi. "Review on modified TiO2 photocatalysis under UV/visible light: selected results and related mechanisms on interfacial charge carrier transfer dynamics." *The Journal of physical chemistry A* 115, no. 46 (2011): 13211-13241. https://doi.org/10.1021/jp204364a

[25] Liao, Hongru, Yu Ran, Junbo Zhong, Jianzhang Li, Minjiao Li, and Hao Yang. "Panax notoginseng powder-assisted preparation of carbon-quantum-dots/BiOCl with enriched oxygen vacancies and boosted photocatalytic performance." *Environmental research* 215 (2022): 114366. https://doi.org/10.1016/j.envres.2022.114366

[26] Liu, Chenhan, Chao Wu, Yunshan Zhao, Zuhuang Chen, Tian-Ling Ren, Yunfei Chen, and Gang Zhang. "Actively and reversibly controlling thermal conductivity in solid materials." *Physics Reports* 1058 (2024): 1-32. https://doi.org/10.1016/j.physrep.2024.01.001

[27] Lu, Peng, Xueli Hu, Yujie Li, Yazhou Peng, Meng Zhang, Xue Jiang, Youzhou He, Min Fu, Fan Dong, and Zhi Zhang. "Novel CaCO3/g-C3N4 composites with enhanced charge separation and photocatalytic activity." *Journal of Saudi Chemical Society* 23, no. 8 (2019): 1109-1118. https://doi.org/10.1016/j.jscs.2019.07.002

[28] Mahala, Chavi, Mamta Devi Sharma, and Mrinmoyee Basu. "Type-II heterostructure of ZnO and carbon dots demonstrates enhanced photoanodic performance in photoelectrochemical water splitting." *Inorganic Chemistry* 59, no. 10 (2020): 6988-6999. https://doi.org/10.1021/acs.inorgchem.0c00479

[29] McGlasson, Alex, and Thomas P. Russell. "From solid surfactants to micromotors: An overview of the synthesis and applications of heterogeneous particles." *Materials Today* 74 (2024): 149-166. https://doi.org/10.1016/j.mattod.2024.01.005

[30] Mishra, Saurav, Nandana Chakinala, Anand G. Chakinala, and Praveen K. Surolia. "Photocatalytic degradation of methylene blue using monometallic and bimetallic Bi-Fe doped TiO2." *Catalysis Communications* 171 (2022): 106518. https://doi.org/10.1016/j.catcom.2022.106518

[31] Mondal, Manisha, and Subhamay Pramanik. "A mechanism for excitation-dependent emission from carbon nanodots." *Materials Letters: X* 18 (2023): 100195. https://doi.org/10.1016/j.mlblux.2023.100195

[32] Mostafa, Mohsen M., and Asmaa S. Morshedy. "Novel Calcium Carbonate-titania nanocomposites for enhanced sun light photo catalytic desulfurization process." *Journal of Environmental Management* 250 (2019): 109462. https://doi.org/10.1016/j.jenvman.2019.109462

[33] Ali, Mohamed Mukthar, JS Arya Nair, and K. Y. Sandhya. "Role of reactive oxygen species in the visible light photocatalytic mineralization of rhodamine B dye by P25–carbon dot photocatalyst." *Dyes and Pigments* 163 (2019): 274-284. https://doi.org/10.1016/j.dyepig.2018.11.057

[34] Ong, Wee-Jun, Lling-Lling Tan, Siang-Piao Chai, Siek-Ting Yong, and Abdul Rahman Mohamed. "Surface charge modification via protonation of graphitic carbon nitride (g-C3N4) for electrostatic self-assembly construction of 2D/2D reduced graphene oxide (rGO)/g-C3N4 nanostructures toward enhanced photocatalytic reduction of carbon dioxide to methane." *Nano Energy* 13 (2015): 757-770. https://doi.org/10.1016/j.nanoen.2015.03.014

[35] Prasetyo, Hendri, Muhammad Noorul Anam Mohd Norrdin, Mohd Hafiz Dzarfan Othman, Juhana Jaafar, Tomohisa Yoshioka, Zhan Li, and Mukhlis A. Rahman. "Technologies for treating wastewater from textile industry: a review." *Materials Today: Proceedings* 65 (2022): 3066-3072. https://doi.org/10.1016/j.matpr.2022.04.214

[36] Abd Rani, Umairah, Law Yong Ng, Ching Yin Ng, Ebrahim Mahmoudi, Yee-Sern Ng, and Abdul Wahab Mohammad. "Sustainable production of nitrogen-doped carbon quantum dots for photocatalytic degradation of methylene blue and malachite green." *Journal of Water Process Engineering* 40 (2021): 101816. https://doi.org/10.1016/j.jwpe.2020.101816

[37] Saini, Deepika, Anjali Kumari Garg, Chumki Dalal, Satyesh Raj Anand, Sumit Kumar Sonkar, Amit Kumar Sonker, and Gunnar Westman. "Visible-light-promoted photocatalytic applications of carbon dots: a review." *ACS Applied Nano Materials* 5, no. 3 (2022): 3087-3109. https://doi.org/10.1021/acsanm.1c04142

[38] Saini, Surendra, Krishan Kumar, Pratibha Saini, Dinesh Kumar Mahawar, Kuldeep S. Rathore, Sanjay Kumar, Anshu Dandia, and Vijay Parewa. "Sustainable synthesis of biomass-derived carbon quantum dots and their catalytic application for the assessment of α, β-unsaturated compounds." *RSC advances* 12, no. 50 (2022): 32619-32629. https://doi.org/10.1039/D2RA05201F

[39] Senthilkumaar, S., P. R. Varadarajan, K. Porkodi, and C. V. Subbhuraam. "Adsorption of methylene blue onto jute fiber carbon: kinetics and equilibrium studies." *Journal of colloid and interface science* 284, no. 1 (2005): 78-82. https://doi.org/10.1016/j.jcis.2004.09.027

[40] Soni, Himanshi, Monika Bhattu, Manvinder Kaur, Meenakshi Verma, and Jagpreet Singh. "Recent advances in waste-derived carbon dots and their nanocomposites for environmental remediation and biological applications." *Environmental Research* 251 (2024): 118560. https://doi.org/10.1016/j.envres.2024.118560

[41] Wang, Jiaxin, Bo Gao, Jiajun An, Jiadong Liu, Lei Wang, and Mika Sillanpää. "How does calcium carbonate enhance pollutants degradation under light illumination? Enhanced scattering and hydroxyl radical." *Journal of Environmental Chemical Engineering* 12, no. 2 (2024): 112457. https://doi.org/10.1016/j.jece.2024.112457

[42] Wang, Min, Rui Shi, Manjie Gao, Kailian Zhang, Linlin Deng, Qifeng Fu, Lujun Wang, and Die Gao. "Sensitivity fluorescent switching sensor for Cr (VI) and ascorbic acid detection based on orange peels-derived carbon dots modified with EDTA." *Food chemistry* 318 (2020): 126506. https://doi.org/10.1016/j.foodchem.2020.126506

[43] Wang, Ru, Kang-Qiang Lu, Zi-Rong Tang, and Yi-Jun Xu. "Recent progress in carbon quantum dots: synthesis, properties and applications in photocatalysis." *Journal of Materials Chemistry A* 5, no. 8 (2017): 3717-3734. https://doi.org/10.1039/C6TA08660H

[44] Wang, Zijing, Rahil Changotra, Mita Dasog, Gurpreet Singh Selopal, Jie Yang, and Quan Sophia He. "Carbon quantum dots: Synthesis via hydrothermal processing, doping strategies, integration with photocatalysts, and their application in photocatalytic hydrogen production." *Sustainable Materials and Technologies* 44 (2025): e01386. https://doi.org/10.1016/j.susmat.2025.e01386

[45] Yu, Zhihan, Fang Li, and Quanjun Xiang. "Carbon dots-based nanocomposites for heterogeneous photocatalysis." *Journal of Materials Science & Technology* 175 (2024): 244-257.

[46] Zhao, Wei, Wanhong Ma, Chuncheng Chen, Jincai Zhao, and Zhigang Shuai. "Efficient degradation of toxic organic pollutants with Ni2O3/TiO2-x B x under visible irradiation." *Journal of the American Chemical Society* 126, no. 15 (2004): 4782-4783. https://doi.org/10.1016/j.jmst.2023.08.023